

Noble-gas broadening rates for the $6s^2\ ^1S_0 \rightarrow 6s6p\ ^1,^3P_1$ resonance and intercombination lines of barium

E. Ehrlacher and J. Huennekens

Department of Physics, Lehigh University, 16 Memorial Drive East, Bethlehem, Pennsylvania 18015

(Received 22 October 1992)

The collisional-broadening and -shift rate coefficients (k_{br} and k_{shift}), for both helium and argon buffer gases, have been measured in the impact limit for the $6s^2\ ^1S_0 \rightarrow 6s6p\ ^3P_1$ intercombination transition of barium. Detailed absorption line shapes were measured at three different ground-state number densities by monitoring the transmitted intensity of a weak cw probe laser as it was scanned over the transition. A single, density-independent line shape was then constructed and fit to a sum of Voigt functions (to account for hyperfine structure and isotope shifts) in order to determine the broadening and shift rates. By repeating the process for several buffer-gas pressures, k_{br} and k_{shift} were determined from least-squares straight-line fits to the broadening and shift rates versus buffer-gas number density. Absolute normalization of the line-shape data was used to provide accurate ground-state column densities. Column-density information was then combined with measurements of white-light-absorption equivalent widths for the $6s^2\ ^1S_0 \rightarrow 6s6p\ ^1P_1$ resonance transition to yield broadening rates for that transition. These values for the resonance line lie between previous literature values, which are widely discrepant. Finally we measured the absolute metastable $6s5d\ ^3D_2$ column density under conditions of optical pumping through the 3P_1 level, and determined that, in steady state, even with a weak cw pump laser, $\sim 20\%$ of all barium atoms in the vapor could be found in the 3D_2 level (with approximately 60% spread over the full 3D_J metastable manifold).

PACS number(s): 32.70.Jz

I. INTRODUCTION

In a recent article [1] we reported impact-regime noble-gas (helium and argon) collisional-broadening and -shift rates for transitions out of the barium $6s5d\ ^3D_J$ levels (see Fig. 1). In that work the 3D_J levels were populated through spontaneous and stimulated radiative processes following pumping of the $6s^2\ ^1S_0 \rightarrow 6s6p\ ^3P_1$ intercombination line with a weak cw diode laser. Although we only used 15 mw of pump power in an unfocused beam, we noted that a large fraction of the ground-state atoms could be transferred to the metastable 3D_J levels. However, while the 3D_J level densities could be accurately measured in these detailed line-shape studies, the fraction of ground-state atoms transferred to the metastable levels could not be accurately determined because of uncertainty in our knowledge of the ground-state density. This uncertainty, in turn, was due to an order-of-magnitude discrepancy in literature values of the collisional-broadening rate coefficients k_{br} for the $6s^2\ ^1S_0 \rightarrow 6s6p\ ^1P_1$ resonance transition at 553.5 nm [2–4]. (In Ref. [1] ground-state densities were determined from absorption-equivalent-width measurements on the resonance transition. The uncertainty in densities determined in this fashion directly reflects the uncertainty in these broadening rates.) For example, Refs. [2,3] report a cross section which can be converted to a value of $k_{\text{br}} = (1.60 \pm 0.06) \times 10^{-9} \text{ cm}^3 \text{ sec}^{-1}$ at $T = 940 \text{ K}$ for Ar buffer gas. On the other hand, Ref. [4] reports a half-width-at-half-maximum argon broadening-rate coefficient of $(5.0 \pm 0.5) \times 10^{-9} \text{ cm}^3 \text{ sec}^{-1}$ at 744 K, which

yields $k_{\text{br}} = (1.0 \pm 0.1) \times 10^{-8} \text{ cm}^3 \text{ sec}^{-1}$ for the full-width-at-half-maximum broadening-rate coefficient, which is the parameter we use here. Similar discrepancies exist for the helium case: $(1.74 \pm 0.07) \times 10^{-9} \text{ cm}^3 \text{ sec}^{-1}$ in Ref. [2] compared with $(9.8 \pm 1.0) \times 10^{-9} \text{ cm}^3 \text{ sec}^{-1}$ in Ref. [4].

In the present work we report detailed line-shape measurements for the 791.1-nm $6s^2\ ^1S_0 \rightarrow 6s6p\ ^3P_1$ intercombination line of barium using both helium and argon perturber atoms (see Fig. 1). Both collisional-broadening rate coefficients k_{br} and collisional-shift rate coefficients k_{shift} are obtained. With these results, we can now accurately determine the ground-state barium column density nL at various temperatures in our heat-pipe oven. Absorption-equivalent-width measurements on the $6s^2\ ^1S_0 \rightarrow 6s6p\ ^1P_1$ resonance transition, taken under identical conditions, are then combined with the known column density to yield the argon and helium broadening rates for the resonance transition. This technique, which yields broadening-rate coefficients for the resonance transition that are intermediate to those previously reported, is free of relatively large systematic errors caused by uncertainty in the vapor length, or in the magnitude and spatial variation of the barium density. Finally, by recording full $6s^2\ ^1S_0 \rightarrow 6s6p\ ^3P_1$ and $6s5d\ ^3D_2 \rightarrow 5d6p\ ^3F_3$ transition line shapes under identical conditions, an accurate value of the ratio of 3D_2 metastables to ground-state atoms is determined.

Section II of this paper describes our experimental setup and procedures. The results of our measurements are presented in Sec. III, while a brief discussion of their significance is given in Sec. IV.

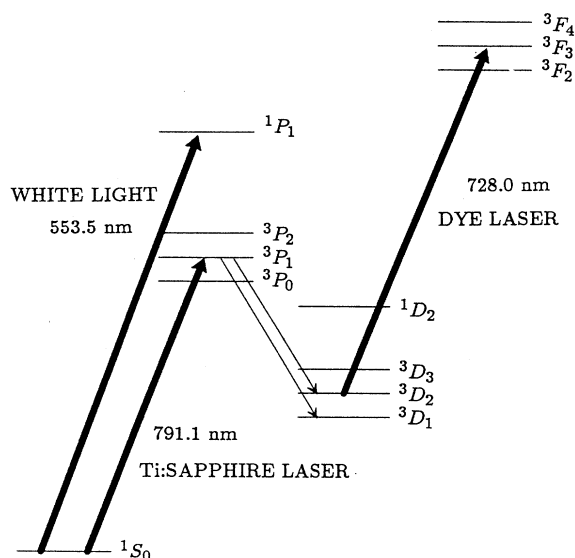


FIG. 1. Energy-level diagram showing the lowest atomic energy levels in barium. The thick arrows represent the three transitions of interest in this work. The thin arrows show the optical-pumping channels for populating the $6s5d\ ^3D_j$ levels through the $6s6p\ ^3P_1$ state. Note that energy splittings are not to scale.

II. EXPERIMENTAL METHODS

Figure 2 shows the experimental setup used to measure the collisional-broadening rate coefficients. This is basically the same experimental setup used in Ref. [1] except that the diode (pump) laser has been replaced by an argon-laser pumped, tunable, single-mode, cw, Ti:sapphire laser (see Fig. 2 caption).

Barium was contained in a five-arm cross heat-pipe oven [5]. The oven was filled with 10–500 Torr of either helium or argon buffer gas and was maintained at a set temperature in the range 765 to 865 K. Since the barium pressure at these temperatures was much below that of the buffer gas, the heat-pipe oven was not operating in the true heat-pipe mode. Ground-state populations were probed in absorption using the Ti:sapphire laser tuned across the $6s^2\ ^1S_0 \rightarrow 6s6p\ ^3P_1$ transition at 791.13 nm. The laser intensity was highly attenuated (down to a few hundred nanowatts) with neutral density filters in order to avoid hyperfine pumping and saturation effects. The transmitted laser intensity was detected with a photomultiplier tube and a lock-in amplifier.

In Ref. [1] we noted that accurate information concerning the absorption coefficient k_ν at frequency ν is best obtained when the absorption at that frequency is between 10% and 90%. In that work we were able to map out a composite absorption line shape (from the core out to the line wings) by varying the density of atoms in the metastable levels. This, in turn, was accomplished by

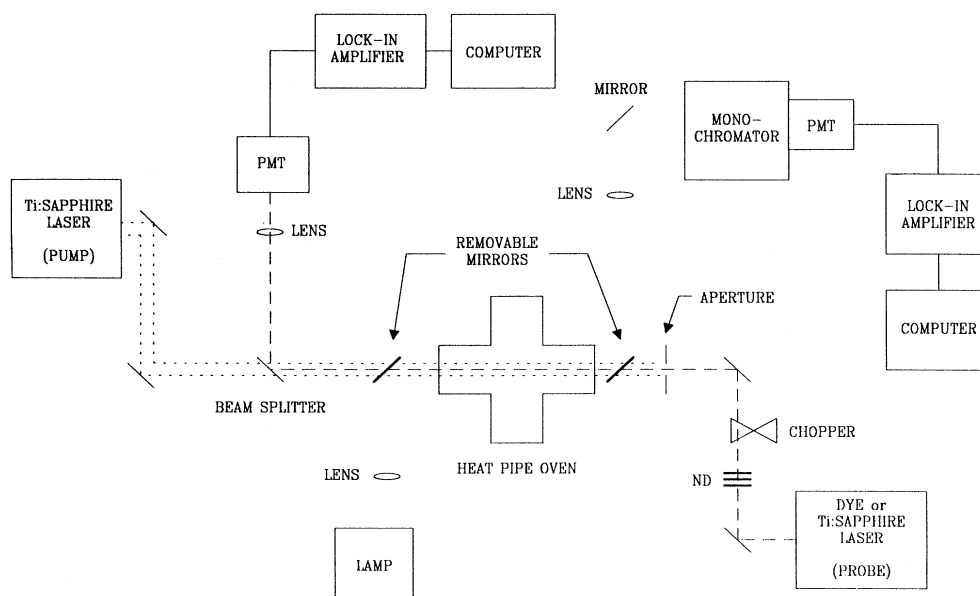


FIG. 2. Experimental setup used for the three types of measurements reported in this work. For measuring broadening and shift rates of the intercombination line at 791.1 nm, only the highly attenuated Ti:sapphire probe laser was used. For studies of the 3D_2 level, the full power (~ 200 mW) of the Ti:sapphire laser was used as the pump, while the highly attenuated dye laser was used as the probe. Finally, for investigations of the resonance transition, the removable mirrors were inserted into the setup and frequency-dependent transmission of the white light was monitored using the monochromator-PMT with all lasers off. PMT and ND represent photomultiplier tube and neutral density filter, respectively.

simply varying the pump-laser power (see Ref. [1]). In the present experiment, we could only change the lower-(ground-) state population by variation of the oven temperature. Thus, the region of the line shape probed by the laser was systematically changed from the core of the line out into the wings by increasing the oven temperature. (Possible systematic errors which arise from the use of temperature to vary density will be discussed later in this article). We obtained laser-absorption line profiles by scanning the laser over the intercombination line. Such scans were recorded at $T = 765, 810, \text{ and } 865 \text{ K}$ and with either helium or argon buffer-gas pressures of 10, 20, 50, 100, 200, and 500 Torr. Composite line shapes were then mapped out using the density scaling method detailed in Sec. III of Ref. [1].

In the second part of this experiment, sequential probe-laser absorption measurements were carried out for the $6s^2\ ^1S_0 \rightarrow 6s6p\ ^3P_1$ intercombination line (using the highly attenuated Ti: sapphire laser as the probe) and for the $6s5d\ ^3D_2 \rightarrow 5d6p\ ^3F_3$ transition (using the full Ti: sapphire pump-laser intensity of $\sim 200 \text{ mW}$ at the heat-pipe entrance window to strongly populate the metastable level). In the latter case, the Ti:sapphire laser was tuned to the center of the $^1S_0 \rightarrow ^3P_1$ intercombination line at 791.1 nm, and a highly attenuated ($\sim 100\text{-nW}$), single-mode, cw dye laser, tuned near 728.0 nm, was used as the probe. Also, white-light absorption of the $6s^2\ ^1S_0 \rightarrow 6s6p\ ^1P_1$ resonance transition was recorded by inserting the removable mirrors shown in Fig. 2 into the beam path and scanning the monochromator near 553.5 nm. Unfortunately, no narrow-bandwidth laser operating in this wavelength region was available to us. Thus we could only measure the total absorption (equivalent width) rather than accurately map out the line-shape function k_ν for the resonance transition. The three measurements were carried out in rapid succession so that conditions in the heat-pipe oven would vary as little as possible. Each of these three scans was taken at 50, 100, 200, and 500 Torr of argon buffer gas for only one heat-pipe temperature, 865 K (and thus only one ground-state number density). The intercombination transition was probed using the method described in the preceding paragraph. The $^3D_2 \rightarrow ^3F_3$ and resonance transitions were probed using the dye laser (with full Ti:sapphire pump-laser power) and the white light (with all lasers blocked), respectively.

III. RESULTS

As stated in Sec. II, composite line shapes were mapped out for the $^1S_0 \rightarrow ^3P_1$ transition for 10, 20, 50, 100, 200, and 500 Torr for both He and Ar buffer gases. A detailed description of how these line shapes are obtained from experimental absorption curves can be found in Sec. III of Ref. [1]. Thus we will give only a brief summary of the procedure here.

The intensity of light of frequency ν that is transmitted through a length L of vapor is given by

$$I_\nu(L) = I_\nu(0) \exp(-k_\nu L), \quad (1)$$

where $I_\nu(0)$ is the incident intensity and k_ν is the absorption coefficient at frequency ν . The absorption coefficient

can be obtained from Eq. (1) as

$$k_\nu = -\frac{1}{L} \ln[I_\nu(L)/I_\nu(0)]. \quad (2)$$

As long as self-broadening can be neglected [which was true in our case where the perturber (buffer-gas) atom density n_p exceeded the barium ground-state density n by more than four orders of magnitude], the absorption coefficient will scale linearly with n . Thus absorption coefficients measured with different ground-state densities can be scaled to each other in their regions of overlap. Reference [1] gives a detailed description of this scaling procedure. After this scaling, we have a single line-shape function k_ν/n in relative units. An absolute scale can be placed on the line profile using the well-known normalization condition [6]

$$\int (k_\nu/n) d\nu = \frac{\lambda^2}{8\pi} \frac{g_2}{g_1} \Gamma_{\text{nat}}, \quad (3)$$

where λ is the wavelength, Γ_{nat} is the transition probability (Einstein A coefficient), and g_2 and g_1 are the upper- and lower-state statistical weights, respectively. Figure 3 shows absolute $6s^2\ ^1S_0 \rightarrow 6s6p\ ^3P_1$ line-shape functions obtained from our experimental data at six argon pressures.

As in Ref. [1], broadening and shift parameters were obtained from fits of calculated line shapes to the experimental data. In each case, the calculated line shape is a composite of several Voigt functions [which are each a numerical convolution of a Gaussian function (due to Doppler broadening) and a Lorentzian function (due to a combination of pressure and natural broadening)]. Here it should be noted that we model the collisional broadening by a Lorentzian line shape as predicted by the impact theory [7]. The impact theory, which yields a Lorentzian line shape regardless of the form of the interaction potentials, is valid for detunings $\Delta\nu \ll (2\pi\tau_d)^{-1}$, where $\tau_d = \rho_0/\bar{v}$ is the collision duration, ρ_0 is the Weisskopf radius, and \bar{v} is the mean relative velocity of the radiating and perturbing atoms [7]. Simple calculations for the $^1S_0 \rightarrow ^3P_1$ transition show that $(2\pi\tau_d)^{-1} \sim 120 \text{ GHz}$ for argon and $\sim 400 \text{ GHz}$ for helium perturbers, and thus the present data, recorded for detunings less than 10 GHz (see Fig. 3), are well within the impact regime. However, barium has several isotopes and the odd mass nuclei have nonzero nuclear spin. Thus, in order to account for both hyperfine structure and isotope shifts, more than one Voigt function was needed to model the full line shape. In the present case, the $6s^2\ ^1S_0 \rightarrow 6s6p\ ^3P_1$ line shape was modeled as a sum of nine Voigt profiles, where isotopes with less than 2% abundance were neglected. Hyperfine constants were obtained from Ref. [8] and isotope shifts from Ref. [9]. In the fits, the only free parameters were the Voigt parameter (usually called "a," which is related to the ratio of the Lorentzian width to the Gaussian width; see Refs. [1] and [10]) and the line-center shift $\Delta\nu_{\text{shift}}$. Since the Gaussian width was fixed by the temperature, the Voigt parameter directly yields the broadening rate $\Gamma_{\text{br}} = k_{\text{br}} n_p$.

By plotting Γ_{br} versus perturber number density n_p ,

the collisional-broadening rate coefficients k_{br} were determined (see Fig. 4). Similarly, we also determined the shift rate coefficients by plotting the collisional line shift $2\pi\Delta\nu_{\text{shift}}$ versus n_p (see Fig. 5). [Since we plotted the frequency of the peak absorption coefficient as measured by the laser wavemeter (which in general contributes a small systematic error), we fit the two line slopes and the single intercept in a global fit of the data of Fig. 5.] Rate coefficients are presented in Table I along with the broadening-to-shift rate ratios. We note that while argon causes a red shift of the line, helium perturbors give rise to a small blue shift.

Next, we look at the argon broadening rate of the $6s^2^1S_0 \rightarrow 6s6p^1P_1$ resonance transition. First, we note that Eq. (3) can be manipulated into a convenient expres-

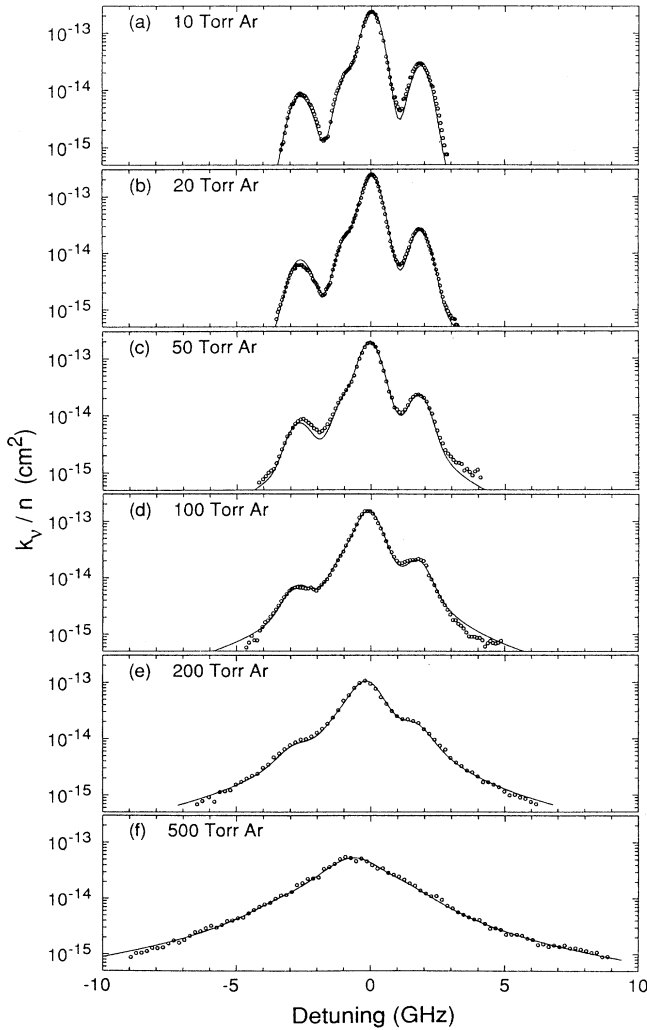


FIG. 3. Comparison of the experimental $6s^2^1S_0 \rightarrow 6s6p^3P_1$ transition line shapes (data points) at various Ar pressures with the composite Voigt line shapes that were calculated using the measured value of k_{br}^{Ar} (solid lines).

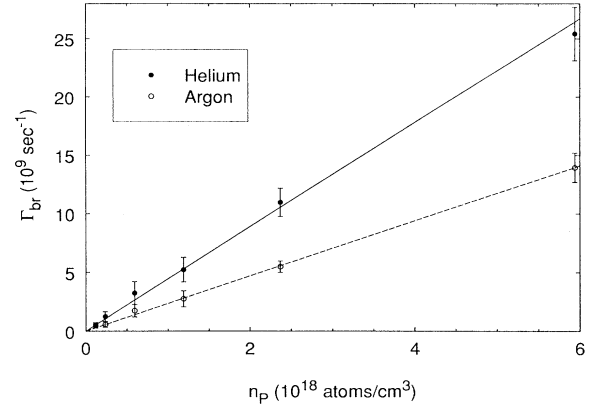


FIG. 4. Plot of Γ_{br} vs perturber density n_p for the 791.1-nm $^1S_0 \rightarrow ^3P_1$ intercombination line using both He and Ar perturber atoms. The solid and dashed lines are the least-squares fits for He and Ar buffer gas, respectively. k_{br} is determined from the slopes of these lines.

sion for the ground-state column density nL .

$$\begin{aligned} nL &= \left[\frac{\lambda^2}{8\pi} \frac{g_2}{g_1} \Gamma_{\text{nat}} \right]^{-1} \int k_\nu L d\nu \\ &= \left[\frac{\lambda^2}{8\pi} \frac{g_2}{g_1} \Gamma_{\text{nat}} \right]^{-1} \int \ln[I_\nu(0)/I_\nu(L)] d\nu, \end{aligned} \quad (4)$$

where the second equality follows from Eq. (2). Thus the quantity nL can be accurately determined from our intercombination-line absorption measurements and known constants. Note that the ground-state density n can also be determined in this manner by simply dividing both sides of Eq. (4) by the vapor length L . However, the error in n is much greater than the error in the column density, since the length of the vapor column in this heat-pipe oven (which is not used in the heat-pipe mode)

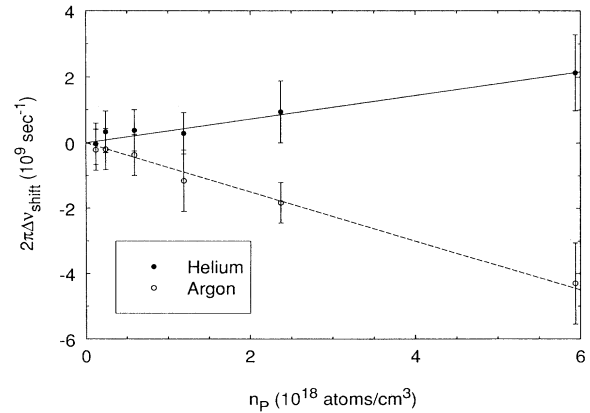


FIG. 5. Plot of collisional line shifts vs n_p for the 791.1-nm $^1S_0 \rightarrow ^3P_1$ intercombination line using both He and Ar perturbors. The solid and dashed lines are the least-squares fits for He and Ar buffer gas, respectively. Slopes of these lines yield k_{shift} .

TABLE I. Ba ($6s^2^1S_0 \rightarrow 6s6p^3P_1$) impact-regime collisional-broadening and -shift rate coefficients (in units of $10^{-9} \text{ cm}^3 \text{ sec}^{-1}$), measured at 810 K.

| Coefficient | Argon | Helium |
|----------------------------------|------------------|------------------|
| k_{br} | 2.35 ± 0.21 | 4.45 ± 0.41 |
| k_{shift} | -0.75 ± 0.16 | $+0.36 \pm 0.17$ |
| $k_{\text{br}}/k_{\text{shift}}$ | -3.1 ± 0.7 | $+12 \pm 6$ |

could not accurately be determined. In essence, the intercombination-line absorption gives a direct measure of the total number of ground-state atoms along the laser path, i.e., the quantity measured is

$$nL \equiv \int_0^L n(x) dx, \quad (5)$$

where n is the average density along the vapor length L . Thus the quantity nL is well determined, even if L is not well known or even if the density is not uniform along the laser path.

Using the white light and monochromator shown in Fig. 2, we measured the total absorption (equivalent width) of the $6s^2^1S_0 \rightarrow 6s6p^1P_1$ resonance transition. The experimental equivalent width (in wavelength units) is defined by the expression [11]

$$W_\lambda = \frac{\lambda^2}{c} \int \frac{I_\nu(0) - I_\nu(L)}{I_\nu(0)} d\nu = \frac{\lambda^2}{c} \int [1 - \exp(-k_\nu L)] d\nu, \quad (6)$$

where the second equality follows from Eq. (1).

For a pressure-broadened line in the impact limit, it can be shown that the equivalent width is given by [6,11]

$$W_\lambda = \frac{\lambda^2}{c} \left[\frac{\lambda^2}{8\pi^2} \frac{g_2}{g_1} \Gamma_{\text{nat}} nL \Gamma_{\text{br}} \right]^{1/2}, \quad (7)$$

where it has been assumed that $\Gamma_{\text{br}} \gg \Gamma_{\text{nat}}$ and $\Gamma_{\text{br}} \gg 2\pi\Delta\nu_D$ (with $\Delta\nu_D$ being the Doppler width of the transition). nL was taken from the intercombination-line absorption measurements as described above, and a value for the resonance-line foreign-gas collisional-broadening rate $\Gamma_{\text{br}}(\text{Ar})$ was obtained at each argon pressure from the measured resonance-line equivalent width and Eq. (7). Values of $\Gamma_{\text{br}}(\text{Ar})$ and W_λ^{Ar} at each pressure are listed in Table II. The $\Gamma_{\text{br}}(\text{Ar})$ values are also plotted in Fig. 6, from which the slope of the least-squares straight-line fit

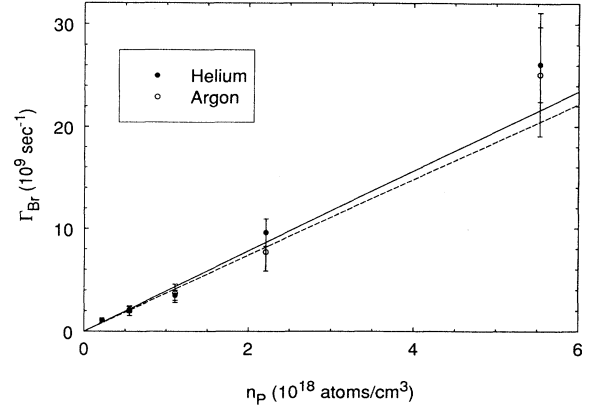


FIG. 6. Plot of Γ_{br} vs n_p (for Ar and He perturber atoms) for the 553.5-nm $^1S_0 \rightarrow ^1P_1$ barium resonance transition. k_{br} values are determined from the slopes of the solid (He) and dashed (Ar) least-squares-fitted lines.

yields the value

$$k_{\text{br}}^{\text{Ar}}(6s^2^1S_0 \rightarrow 6s6p^1P_1) = (3.6 \pm 0.9) \times 10^{-9} \text{ cm}^3 \text{ sec}^{-1} \quad (8)$$

for argon perturbers. Ratios of resonance-line equivalent widths for equal pressures of helium and argon perturbers (see Table II) were used with this argon broadening-rate coefficient to obtain the helium broadening rates $\Gamma_{\text{br}}(\text{He})$ [i.e.,

$$\Gamma_{\text{br}}(\text{He}) = k_{\text{br}}^{\text{Ar}} n_p (W_\lambda^{\text{He}} / W_\lambda^{\text{Ar}})^2$$

from Eq. (7)]. These values are also plotted in Fig. 6, from which we obtain

$$k_{\text{br}}^{\text{He}}(6s^2^1S_0 \rightarrow 6s6p^1P_1) = (3.9 \pm 1.2) \times 10^{-9} \text{ cm}^3 \text{ sec}^{-1}. \quad (9)$$

Finally, we are now in a position to determine the fraction of the ground-state atoms that were pumped into the metastable $6s5d^3D_j$ levels through optical pumping by the 200-mW cw Ti:sapphire laser tuned to the $6s^2^1S_0 \rightarrow 6s6p^3P_1$ transition. In our low-power probe of the intercombination line with the Ti:sapphire laser, we measured the ground-state column density nL as described above. Similarly, our low-power dye-laser probe of the $6s5d^3D_2 \rightarrow 5d6p^3F_3$ transition (counter propaga-

TABLE II. Ba ($6s^2^1S_0 \rightarrow 6s6p^1P_1$) resonance-line absorption equivalent widths and broadening rates.

| Pressure (Torr) | W_λ^{Ar} (Å) | $\Gamma_{\text{br}}(\text{Ar})$ (10^9 sec^{-1}) | $W_\lambda^{\text{He}} / W_\lambda^{\text{Ar}}$ | $\Gamma_{\text{br}}(\text{He})$ (10^9 sec^{-1}) |
|-----------------|-----------------------------|---|---|---|
| 20 | | | 1.17 ± 0.13 | 1.1 ± 0.2 |
| 50 | 0.79 ± 0.04 | 2.0 ± 0.5 | 1.01 ± 0.07 | 2.1 ± 0.4 |
| 100 | 1.06 ± 0.05 | 3.7 ± 0.9 | 0.94 ± 0.07 | 3.5 ± 0.6 |
| 200 | 1.51 ± 0.08 | 7.7 ± 1.8 | 1.09 ± 0.08 | 9.6 ± 1.7 |
| 500 | 2.27 ± 0.11 | 25.1 ± 6.0 | 1.14 ± 0.08 | 26.1 ± 4.7 |

TABLE III. Ground and metastable 3D_2 level densities in optically pumped barium vapor.

| P_{Ar} | $n(^1S_0)^a$ (10^{12} cm^{-3}) | $n(^3D_2)^b$ (10^{12} cm^{-3}) | $n(^3D_2)/n(^1S_0)$ (%) |
|----------|---|---|----------------------------|
| 50 | 10.8 ± 3.5 | 2.08 ± 0.62 | 19 ± 5 |
| 100 | 10.4 ± 3.3 | 2.61 ± 0.78 | 25 ± 7 |
| 200 | 10.3 ± 3.3 | 2.16 ± 0.64 | 21 ± 6 |
| 500 | 7.1 ± 2.3 | 1.74 ± 0.52 | 24 ± 7 |

^aGround-state density from $^1S_0 \rightarrow ^3P_1$ low-power Ti:sapphire laser absorption.

^b 3D_2 density from $^3D_2 \rightarrow ^3F_3$ dye-laser absorption, following pumping on the $^1S_0 \rightarrow ^3P_1$ transition with 200 mW of Ti:sapphire laser power.

ting with the unattenuated Ti:sapphire beam) measured the metastable-level column density $n_{^3D_2} L$ from an expression analogous to Eq. (4). Thus the fraction of ground-state atoms pumped into the 3D_2 state ($n_{^3D_2}/n$) is given directly by the ratio of these two values. These fractions, which also are not affected by errors in the vapor length or spatial gradients in the ground-state density, are given in Table III for four argon pressures and a temperature of 865 K. Absolute ground and 3D_2 level densities at each pressure can be calculated by dividing the column densities by $L = 20$ cm. These values are also given in Table III.

IV. DISCUSSION

As stated in Sec. II, construction of the composite line shapes required us to vary the barium ground-state density by changing the heat-pipe oven temperature. This might seem to present a problem since important quantities such as the pressure-broadening rate Γ_{br} and the Doppler width $\Delta\nu_D$ are temperature dependent. However, in our analysis we assumed a constant temperature, which we chose to be 810 K (the middle temperature of the three studied in this work). With this approximation, these temperature-dependent quantities are either overestimated (at 865 K) or underestimated (at 765 K), but by no more than 3%. We therefore used this approximation, which greatly simplified the analysis, since uncertainties in the scaling and fitting were already larger than 3%. (See Sec. IV of Ref. [1] for a detailed discussion of these other uncertainties.) Thus, the values of k_{br} reported here in Table I for the intercombination line should be considered to be valid for 810 K. It is expected that k_{br} should follow a $T^{0.3}$ temperature dependence in the limit of pure van der Waals broadening [12], although this point was not tested here.

Overall uncertainties in the intercombination-line

broadening and shift coefficients are therefore similar to those reported in Ref. [1] for the analogous coefficients in the transitions from the metastable levels, and these uncertainties are listed with our present results in Table I. We note that, similar to the results of Refs. [1] and [13], the ratio of linewidth to line-center shift is -3.1 ± 0.7 for argon buffer gas (which is consistent with the value -2.8 expected for pure van der Waals broadening), while the same ratio is $+12 \pm 6$ for helium perturbers (which indicates that the short-range potentials are much more important in this case and that the broadening clearly cannot be described by a pure R^{-6} interaction).

In our determination of the resonance-line argon broadening rate, we used the approximate expression, Eq. (7), for the equivalent width. While this expression is certainly valid at high buffer-gas pressures where $\Gamma_{br} \gg \Gamma_{nat}$ and $\Gamma_{br} \gg 2\pi\Delta\nu_D$, the latter inequality is not satisfied at the lower pressures used in this work. However, the equivalent width is dominated by the region of the line profile where the optical depth is approximately unity ($k_\nu L \sim 1$). This is because photons with frequencies in the line core are almost 100% absorbed, regardless of the details of the line shape in that region. Thus, the relevant criterion is not whether $\Gamma_{br} \gg 2\pi\Delta\nu_D$, but whether pressure broadening dominates the region of the line profile near the unity optical-depth points. This condition was tested by calculating resonance-line equivalent widths using the full integral form [Eq. (6)] and a composite line shape consisting of nine Voigt functions (to account for hyperfine structure and isotope shifts). Here the resonance-line hyperfine-structure and isotope-shift constants were taken from Ref. [14]. Since k_ν is a function of Γ_{br} , we could vary Γ_{br} inside the integral in Eq. (6) until the experimental value of W_λ was obtained. With this technique, we obtained values of Γ_{br} which agreed with those found from the simpler closed-form expression [Eq. (7)] to within 3% at 50 Torr of argon and to better than

TABLE IV. Barium $6s^2^1S_0 \rightarrow 6s6p^1P_1$ resonance-line broadening-rate coefficients k_{br} for helium and argon perturbers.

| Reference | k_{br}^{He} ($10^{-9} \text{ cm}^3 \text{ sec}^{-1}$) | k_{br}^{Ar} ($10^{-9} \text{ cm}^3 \text{ sec}^{-1}$) |
|--------------------------------------|--|--|
| Present work | 3.9 ± 1.2 | 3.6 ± 0.9 |
| Zhuvikin, Penkin, Shabanova [2,3] | 1.74 ± 0.07 | 1.60 ± 0.06 |
| Kuchta <i>et al.</i> [4] | 9.8 ± 1.0 | 10.0 ± 1.0 |

1% at 500 Torr.

With the uncertainty in the column density estimated to be $\sim 22\%$ [due mostly to the uncertainty in Γ_{nat} for the intercombination line; see Eq. (4)] and the uncertainty in the measurement of W_λ ($\sim 5\%$), we obtain an overall uncertainty of 25–30% in our values for the $6s^2\ ^1S_0 \rightarrow 6s6p\ ^1P_1$ resonance-line broadening-rate coefficients due to argon and helium perturbers. These values of $k_{\text{br}}^{\text{Ar}} = (3.6 \pm 0.9) \times 10^{-9} \text{ cm}^3 \text{ sec}^{-1}$ and $k_{\text{br}}^{\text{He}} = (3.9 \pm 1.2) \times 10^{-9} \text{ cm}^3 \text{ sec}^{-1}$, which should be considered to be valid for $T = 865 \text{ K}$, fall between the two previously published sets of values which we found in the literature [2,4] and which are listed in Table IV. The three sets of values (including the present work) all disagree within stated error bars, and we are unable to explain the discrepancy at present. However, we have confidence in our present values due to the absence of any significant source of systematic error other than the value of Γ_{nat} for the intercombination line. (In this work we have used the value $\Gamma_{\text{nat}}(6s^2\ ^1S_0 \rightarrow 6s6p\ ^3P_1) = (2.98 \pm 0.45) \times 10^5 \text{ s}^{-1}$ from Ref. [15]. However, if a more accurate value for this parameter is found in the future, our values of $k_{\text{br}}^{\text{Ar}}$ and $k_{\text{br}}^{\text{He}}$ for the resonance line [Eqs. (8) and (9)] can be corrected by simply multiplying our present results by $[\Gamma_{\text{nat}}(\text{new})/\Gamma_{\text{nat}}(\text{Ref. [15]})]_{1S_0 \rightarrow 3P_1}$. Among other reasons, accurate values of these broadening rates are useful in that they allow rapid determination of the metal-atom number densities in a wide range of laboratory barium vapors through simple absorption measurements.

As stated earlier, the fraction of atoms pumped to the metastable 3D_2 level [i.e., the ratio of the 3D_2 atom density (with 200-mW Ti:sapphire laser pumping) to the ground-state density (with the Ti:sapphire laser blocked)] is independent of the vapor length L , which is the most uncertain parameter in the experiment. The principal sources of uncertainty in these ratios come instead from the normalization (which depends on the Γ_{nat} values for the various transitions) and the absorption coefficient scaling. Consequently, we have measured these ratios with an overall uncertainty of $\sim 28\%$. In this manner we found that about 20% of the atoms were excited to the 3D_2 metastable level with 200-mW pump power. From Ref. [1] we know that population is spread roughly equally over the 3D_J levels at these pressures, so that roughly 60% of the atoms would populate these metastable levels under our present conditions. We can now also calibrate our previous work with the weak diode laser (Ref. [1]) and report that $\sim 50\%$ of the atoms were pumped into the metastable levels with only 15 mW of laser power. In

TABLE V. Barium number densities (in units of 10^{13} cm^{-3}) calculated from various vapor pressure formulas at 865 K.

| Reference | n |
|------------------------------------|-------------|
| Present work | (0.71–1.08) |
| Nesmeyanov [18] | 6.36 |
| Bohdansky and Schins [19] | 1.76 |
| Alcock, Itkin, and Horigan [20] | 3.16 |

principle, 100% could be optically pumped to the metastable levels, except for the effects of diffusion into, and out of, the pump beam. We note that Carlsten [16] observed $\sim 78\%$ of ground-state atoms transferred to the metastable 3D_J levels using pulsed laser pumping.

Absolute densities in either the ground or metastable levels (Table III) were not obtained with the same accuracy with which we can determine column densities. This is due to the high uncertainty of the vapor length L . We determined the vapor length to be $L = 20 \pm 5 \text{ cm}$ where the large uncertainty is due to the fact that the oven was not operating in the heat-pipe mode, and the density profile within the oven was not well known. It is possible that more accurate values could be obtained in either a glass cell, or a stainless-steel cell with hot metal o-ring window seals [17]. In either case the cell could be connected to a vacuum and gas handling system for variation of the type and amount of buffer gas. Nevertheless, ground- and metastable-state densities at 865 K and various argon pressures, obtained in this work, are listed in Table III with uncertainties. It is interesting to note that the ground-state densities we measured differ significantly from those obtained from various published barium vapor pressure formulas (which also disagree with each other) [18–20]. A comparison of these values is given in Table V, where it can be seen that our data are most consistent with the formula of Bohdansky and Schins [19]. However, since temperature was not varied in the present experiment, and the oven environment was not in thermal equilibrium, the present data should not be used to critically evaluate the various vapor pressure formulas.

ACKNOWLEDGMENTS

We gratefully acknowledge financial support for this work provided by the National Science Foundation (Grant No. PHY-9119498) and the U.S. Army Research Office (Grant No. DAAL03-89-K-0171).

- [1] E. Ehrlacher and J. Huennekens, *Phys. Rev. A* **46**, 2642 (1992).
 [2] N. P. Penkin and L. N. Shabanova, *Opt. Spektrosk.* **25**, 795 (1968) [*Opt. Spectrosc. (USSR)* **25**, 446 (1968)].
 [3] G. V. Zhuvikin, N. P. Penkin, and L. N. Shabanova, *Opt. Spektrosk.* **46**, 1135 (1979) [*Opt. Spectrosc. (USSR)* **46**, 642 (1979)].

- [4] E. Kuchta, R. J. Alvarez, Y. H. Li, D. A. Krueger, and C. Y. She, *Appl. Phys. B* **50**, 129 (1990).
 [5] C. R. Vidal and J. Cooper, *J. Appl. Phys.* **40**, 3370 (1969).
 [6] A. C. G. Mitchell and M. W. Zemansky, *Resonance Radiation and Excited Atoms* (Cambridge University Press, Cambridge, 1934).
 [7] H. G. Kuhn, *Atomic Spectra* (Academic, New York, 1969).

- [8] G. zu Putlitz, *Ann. Phys. (Leipzig)* **11**, 248 (1963).
- [9] P. Grundevik, M. Gustavsson, G. Olsson, and T. Olsson, *Z. Phys. A* **312**, 1 (1983).
- [10] D. G. Hummer, *Mem. R. Astron. Soc.* **70**, 1 (1965).
- [11] A. Corney, *Atomic and Laser Spectroscopy* (Clarendon, Oxford, 1977).
- [12] N. Lwin, D. G. McCartan, and E.L. Lewis, *Astrophys. J* **213**, 599 (1977).
- [13] M. Kötteritzsch, W. Gries, and A. Hese, *J. Phys. B* **25**, 913 (1992).
- [14] P. E. G. Baird, R. J. Brambley, K. Burnett, D. N. Stacey, D. M. Warrington, and G. K. Woodgate, *Proc. R. Soc. London Ser. A* **365**, 567 (1979).
- [15] W. H. Parkinson and F. S. Tomkins, *J. Opt. Soc. Am.* **68**, 535 (1978).
- [16] J. L. Carlsten, *J. Phys. B* **7**, 1620 (1974).
- [17] J. Huennekens and A. Gallagher, *Phys. Rev. A* **28**, 238 (1983).
- [18] A. N. Nesmeyanov, *Vapour Pressure of the Elements* (Academic, New York, 1963).
- [19] J. Bohdanský and H. E. J. Schins, *J. Phys. Chem.* **71**, 215 (1967).
- [20] C. B. Alcock, V. P. Itkin, and M. K. Horrigan, *Can. Metallurg. Quart.* **23**, 309 (1984).